AFRL-AFOSR-VA-TR-2020-0093

The Development of Efficient and Intelligent Algorithms for a New Class of Multifunctional Reconfigurable Antenna Systems
antenna systems

Bedri Cetiner
UTAH STATE UNIVERSITY

12/06/2019
Final Report

Air Force Research Laboratory
AF Office Of Scientific Research (AFOSR)/ RTA2
Arlington, Virginia 22203
Air Force Materiel Command

REPORT DOCUMENTATION PAGE

Form Approved
OMB No. 0704-0188

1. REPORT DATE *(DD-MM-YYYY)*	2. REPORT TYPE	3. DATES COVERED *(From - To)*
14-07-2020	Final Performance	15 Dec 2014 to 14 Sep 2019

4. TITLE AND SUBTITLE
The Development of Efficient and Intelligent Algorithms for a New Class of Multifunctional Reconfigurable Antenna Systems antenna systems

5a. CONTRACT NUMBER

5b. GRANT NUMBER
FA9550-15-1-0040

5c. PROGRAM ELEMENT NUMBER
61102F

6. AUTHOR(S)
Bedri Cetiner

5d. PROJECT NUMBER

5e. TASK NUMBER

5f. WORK UNIT NUMBER

7. PERFORMING ORGANIZATION NAME(S) AND ADDRESS(ES)
UTAH STATE UNIVERSITY
2400 OLD MAIN HILL
LOGAN, UT 84322-0001 US

8. PERFORMING ORGANIZATION REPORT NUMBER

9. SPONSORING/MONITORING AGENCY NAME(S) AND ADDRESS(ES)
AF Office of Scientific Research
875 N. Randolph St. Room 3112
Arlington, VA 22203

10. SPONSOR/MONITOR'S ACRONYM(S)
AFRL/AFOSR RTA2

11. SPONSOR/MONITOR'S REPORT NUMBER(S)
AFRL-AFOSR-VA-TR-2020-0093

12. DISTRIBUTION/AVAILABILITY STATEMENT
A DISTRIBUTION UNLIMITED: PB Public Release

13. SUPPLEMENTARY NOTES

14. ABSTRACT
In this term, we have focused on the consolidation of the discoveries and designs from previous year's outcome and the development of efficient algorithms to design and utilize MRA and MRA array systems with a large number of modes. In addition, we have explored advanced topics such as the application of machine learning techniques on multifunctional reconfigurable antenna (MRA) design and configuration, and efficient array calibration methods for MRA arrays.
A fundamental requirement for a broad range of communication services is the protection of the privacy of the data being exchanged among transmitter and receivers. In particular, nodes communicating over wireless channels are easy targets for eavesdropping due to inherent broadcast nature of the communi- cation medium. Therefore, physical layer security (PLS) is an essential ingredient of the system design. In this term, we developed novel PLS methods that can utilize MRAs to achieve improved security. We have shown that MRAs can be employed to randomize the channel so that the attacker or jammer signals can be nulled or cancelled. In addition, we extended the typical wiretap channel to a multi-user MIMO communication (MU-MIMO) system where multiple legitimate receivers and eavesdroppers exist. It is seen that with MRAs at the transmitter and legitimate receivers,...

15. SUBJECT TERMS
Algorithms, Antenna, Reconfigurable, Multifunctional

16. SECURITY CLASSIFICATION OF:			17. LIMITATION OF ABSTRACT	18. NUMBER OF	19a. NAME OF RESPONSIBLE PERSON
a. REPORT	b. ABSTRACT	c. THIS PAGE			NGUYEN, TRISTAN

Unclassified	Unclassified	Unclassified	UU	**PAGES**	**19b. TELEPHONE NUMBER** *(Include area code)* 703-696-7796

Progress Report

AFOSR Grant#: FA 9550-15-1-0040 DEF

Title: The Development of Efficient and Intelligent Algorithms for a New Class of MRA Systems

Report Type	Final Report
Primary Contact Email	bedri.cetiner@usu.edu
Primary Contact Phone Number	(435) 797-3320
Organization/Insitution name	Utah State University
Grant/Contract Title	The Development of Efficient and Intelligent Algorithms for a New Class of MRA Systems
Grant/Contract Number	FA9550-15-1-0040
Principle Investigator Name	Bedri Cetiner
Program Manager	Tristan Nguyen
Reporting Period Start Date	12/15/2014
Reporting Period End Date	9/14/2019

Summary

In this term, we have focused on the consolidation of the discoveries and designs from previous year's outcome and the development of efficient algorithms to design and utilize MRA and MRA array systems with a large number of modes. In addition, we have explored advanced topics such as the application of machine learning techniques on multifunctional reconfigurable antenna (MRA) design and configuration, and efficient array calibration methods for MRA arrays.

A fundamental requirement for a broad range of communication services is the protection of the privacy of the data being exchanged among transmitter and receivers. In particular, nodes communicating over wireless channels are easy targets for eavesdropping due to inherent broadcast nature of the communication medium. Therefore, physical layer security (PLS) is an essential ingredient of the system design. In this term, we developed novel PLS methods that can utilize MRAs to achieve improved security. We have shown that MRAs can be employed to randomize the channel so that the attacker or jammer signals can be nulled or cancelled. In addition, we extended the typical wiretap channel to a multi-user MIMO communication (MU-MIMO) system where multiple legitimate receivers and eavesdroppers exist. It is seen that with MRAs at the transmitter and legitimate receivers, the MRA states can be selected to maximize the quality of legitimate reception while achieving a vanishingly small information leakage towards the eavesdroppers. To achieve this, a polarization-and-radiation pattern hoping method has been developed where MRA states can be hopped in a pseudo-random manner (agreed among legitimate nodes) and thus prevents eavesdropper from capturing and decoding the signals. In another task of this term, we investigated the use of machine learning methods for MRA mode selection. Observing that the wireless medium and MRA state jointly determine the channel realizations, we developed online learning techniques that can predict the multi-path medium's state and the MRA states that can create wireless links with higher channel capacities. The procedures for initial and periodic training have been developed to improve channel estimation quality and determine preferred MRA modes while maintaining low training overhead. The developed techniques are on-line and are capable of dynamically adopting to changing medium and tuning the MRA states in conjunction with the overall channel realization history. Yet another study of this term has been the development of efficient calibration techniques for MRA arrays. As is well known, an array of antennas must be calibrated to benefit from beamforming gains. Since MRAs provide enhanced system capabilities via their hardware reconfigurability features, the MRA states may require calibration in addition to the calibration of legacy RF/antenna feed network. In this work, we develop a hierarchical training method that combines array level and MRA element level calibration. To reduce the training overhead for element level calibration, we design a sub-set training method where MRA modes with similar parasitic layer geometries are treated similarly as they are likely to create similar insertion behaviour to the RF-antenna feed circuitry. In this term, we also continued our investigations on the massive hybrid analog-digital MRA arrays where we developed a genetic-algorithm based optimization framework to determine the best MRA array geometry consisting of a small number of full RF-chains that are connected to phase-shifter lines feeding the MRAs thorough adder modules. Observing that the overall transmission can be expressed as multiple of three matrices representing the analog and digital precoding sections, we solved the optimization problem where the objective is to create a desired radiation pattern profile using the MRA modes, phase shifters and selective amplitude tapering.

The antenna designs of this term focused on creating very high-gain MRAs and the investigation of non-ideal effects on MRA performance. A very-high gain MRA, of which can maintain the gain over a large bandwidth, has been achieved by a novel multi-level parasitic layer approach where each parasitic layer

is optimized to provide highest bandwidth with highest uniform gain across its bandwidth. A prototype of this design has been fabricated and measured where the integrity of the antenna was observed to maintain over (3.2-4.2) Ghz, e.g., a 1 GHz bandwidth. In another study, we investigated the impact of non-ideal conditions on the MRA performance, and in particular, we looked into the PIM and EVM performance. The overall results showed that the parasitic pixel layer approach in implementing MRAs is an effective approach as the degradation in EVM and PIM due to parasitic pixel layer switches is minimal. Lastly, in this term, we explored the opportunities of using machine learning techniques to design MRAs. Since solving Maxwell equations for each and every MRA state is a cumbersome procedure, we attempted to develop a artificial neural network that can be trained by a subset of E-field pattern training set generated by solving Maxwell equations and based on this training, can predict the E-field pattern of other MRA states. We are currently investigating the E-field attributes to compress information to associate parasitic layer geometry to E-field pattern.

1 Introduction

This project aims to develop effective solutions to wireless communication systems employing multifunctional and reconfigurable antenna (MRA) technology. The overall activity involves two major thrusts in the form of theory and antenna design.

1. Theory: This project puts a special emphasis on establishing a unified framework between MRA systems and adaptive signal processing techniques with the goal of maximizing the ability of MR-MIMO systems performing highest-level intelligent functionalities, in constantly changing environments due to mobility, propagation and multi-path conditions, and interference. This unified framework will enable the interplay between MRA design and intelligent algorithms, where they feed back to each other, facilitating new design principles, and thereby leading to significant advances in adaptive wireless communication systems.

2. Antenna design: The novelty of the proposed MRAs stems from the effective integration of innovative device designs and operational techniques, and the use of smart materials. This multifaceted approach results in MRAs having highly agile reconfiguration capabilities with low-cost and -size along with reliable operation.

In the following, we provide the final project report along with the progress during the period Dec/2018-Sep/2019.

2 Summary of Work 2014-2018

During the coarse of this project, significant progress has been achieved on the design, optimization and utilization of MRA systems for a broad range of wireless technologies ranging from 5G and beyond wireless communications to tactical radar systems, and secure communications.

In the first year (2014-2015) of this project, we first developed an accurate spatial channel model specific for MRA systems by extending the spatial channel models available from 3GPP project. Relaying on this accurate model, we designed efficient channel estimation techniques to make the MRA systems useful for practical systems as the knowledge of channel estimation is essential for almost all communications systems. Our innovative approach made it possible to utilize a large set of MRA states with relatively small overhead for estimating the channel. In this term, we also looked into direction finding problem using MRA arrays. We have shown that with proper mode selection and spatial smoothing, we can significantly improve the direction finding capability of an array. This result is essential for the radar systems, and in particular, for tactical communications where it is essential to locate the directions of signals from enemy. In the first year, we also developed various MRA systems that created significant breakthrough in frequency and spatial configurable MRA designs. In particular, the 360 degrees reconfigurable array using simple dipole surrounded by a cylindrical parasitic layer has received significant attention from both academia and industry.

Maturing our knowledge and expertise in MRA systems, second year (2015-2016) of the project has witnessed even more breakthrough progress. We initiated a new research path on utilizing the MRA systems for spatial modulation systems. By jointly optimizing the MRA element properties and the array processing, we achieved superior performance with mode-shift keying and mode-modulation schemes.

We extended the use of MRAs for multi-user MIMO systems and have shown that the MRA array systems can significantly increase the number of jointly served users on the same spectral channel by properly modifying the wireless channel through playing with MRA states. Furthermore, we have developed interference alignment schemes for reconfigurable MIMO systems that significantly improved the overall system capacity even with a small number of MRA states made available. Iterative mode selection and interference alignment scheme developed during these efforts attained very good performance with very low complexity. We also developed interference alignment for multi-user single input single output (SISO) systems experiencing significant interference. We have shown that the capacity by treating noise as interference schemes can be significantly improved by allowing MRA elements at each user. In addition to these, we also started to work on massive MIMO systems during this year. We first investigated the capacity of massive MRA arrays in the limiting cases where number of MRA elements and number of users go to infinity but the ratio of MRA number to users is fixed. We calculated the overall gain from using L modes and show that we have logarithmic SNR gain as number of MRA modes per antenna.

The MRA design part of our research during the (2015-2016) term also focused on innovative designs. We have improved the 3D parasitic layer design from first year's outcome, and investigated its performance in 5G networks. Next, we developed a bandwidth reconfigurable patch MRA that is capable of 3D beam-steering. Such MRA design is most useful for cognitive radio systems where various frequency channels are available and the designed single element can perform beamforming in each supported band. This year also coined our progress in mmWave systems. We developed an MRA for 28 GHz, fabricated it along with PCB control lines and control circuitry, and demonstrated that similar beam-steering capabilities can be achieved as we had attained for sub-6 GHz designs. The 28 GHz band has received significant attention from industry and it is expected that this outcome of this project will benefit the leadership of US in 5G wireless technology business around the globe. In addition to 28 GHz MRA, we also fabricated a 60 Ghz MRA that uses phase change materials. In this band, using PIN diode technology is quite cumbersome, and we resorted to nano-technology PCB design techniques to create switches based on phase-change material. This effort can be viewed as a first step towards the engagement of material science and MRA technology for future systems.

In the third year (2016-2017), main focus of the research has been on the development of novel space-time transmission schemes for massive multifunctional reconfigurable multiple-input multiple output (MR-MIMO) antenna systems and the multifunctional reconfigurable antenna (MRA) design optimized for those schemes. In addition, we investigated the use and design of MRA systems for spectrum sharing environments. System level performance analysis have also been conducted to determine the impact of MRA systems on large-scale systems. For massive MIMO systems, the cost of RF chains is the main bottleneck for cost. To reduce the complexity, we extended the idea of constant modulus precoding schemes to MRA arrays that combine simple phase-shifter based precoding with the MRA configuration capability while retaining the performance. The success of this approach relies on the intrinsic gain control capability due to the availability of multiple radiation patterns at each element. In another task, we revisited the MRA case where a large number of modes are employed and one needs to estimate the channel for each mode. We developed a dynamic mode grouping scheme that utilizes the estimation/prediction based channel estimation we introduced in the previous term. The system level performance analysis studies conducted in this term includes the theoretical evaluations of the statistical distribution long-term signal-to-noise ratio at some random location covered by a heterogenous system of wireless access points employing MRAs. For a large-scale wireless system, numerical examples indicate that the geometry can be significantly improved by suitable mode optimization at access points. Another system level design effort has been done to extend network slicing concept to physical layer slicing for

radio access networks equipped with MRA systems. We have so far formulated the impact of MRAs on the key performance indicators (KPIs) of slices required over the air-interface from an access point (AP) to all its users. The MRA designs performed in this term includes 4 different use-cases: (i) A bandwidth and pattern reconfigurable MRA element for CBRS band, (ii) a beam-width and beam-steering controllable MRA element with a small number of switches, (iii) MRA design for MU-MIMO operation, and (iv) MRA array at 5 GHz band. Each of these designs are suitable for extensive set of wireless communication applications.

Finally, in the fourth year (2017-2018) of this project, we conducted investigations on the development of novel space-time transmission schemes for massive MR multiple-input multiple output (MR-MIMO) antenna systems and the MRA design optimized for those schemes. In addition, we investigated the use and design of MRA systems for spectrum sharing, 5G RAN and radar networks. In order to reduce the cost of massive MRA arrays, we consolidated our earlier design and extended them to double hybrid arrays where a low-cost radio distribution network is employed to dynamically assign a small number of full-complexity RF chains to a subset of constant-modulus RF branches employing only phase shifters. We also studied the use of machine learning techniques that can associate temporal and spectral variations to channel & scheduling variations and enables a dynamic mode switching. The dynamic wireless coverage capabilities of MRA systems have also been studied in this term. For radar networks, we studied the use of radar network coverage for a passive radar system in which RA elements can be optimized along with the radar location to create a trade-off between various radar functionalities. In addition, we extended the use of RAs for Treating Interference as Noise (TIN) schemes that have been developed in the past year to the spectrum sharing systems. In this term, we also studied the achievable rates of MIMO systems with RA elements. We modeled the RE-MIMO channel as a compound channel and based on statistical fading channel models, we derived the achievable rate expressions for such channels. We also investigated the capacity limits of a double-layer spatial modulation scheme that has been studied in the previous terms. The MRA design and fabrication in this term has also focused on to support the proposed algorithms as well as to develop novel MRA design techniques. A horn-antenna based MRA has been designed and analyzed for X-band (8-12 GHz). This MRA targets the satellite communication applications and can be utilized to improve communication reliability for tactical systems as well. In another design, we developed a parasitic layer based reconfigurable antenna (RA) that targets sub-6 GHz spectrum sharing applications and is capable of dynamically changing its impedance bandwidths between narrow and broad frequency bands (3.4-3.6 GHz & 3.1-3.9 GHz) and can concurrently steer its main radiation beam into three different directions. This design is especially important for the TIN scheme that has been investigated for spectrum sharing environments as it can create various directional modes across a wide range of spectrum. In this term, we also initiated a research area on the use of graphene based switching technologies for MRA designs.

Based on our extensive foundation developed throughout the four fruitful years of this project, we continued our efforts in the 2018/2019 term. In the following, we summarize the outcome of the progress achieved through 2018-2019 term.

3 Summary of Work Done 2018-2019

3.1 Algorithm Development for MRA Systems

3.1.1 Enhanced Physical Layer Security via Channel Randomization with Reconfigurable Antennas

Secure wireless communication techniques based on physical (PHY) layer properties are promising alternatives or complements to traditional upper- layer cryptography-based solutions, due to the capability of achieving message confidentiality or integrity and authentication protection without pre-shared secrets. While many theoretical results are available, there are few practical PHY-layer security schemes,mainly because the requirement of channel advantage between the legitimate users versus the attacker's is hard to satisfy in all cases. Recent research shows that channel randomization, which pro-actively and dynamically perturbs the physical channel so as to create an artificial channel advantage, is helpful to enhance certain PHY-layer security goals such as secrecy. However, a systematic study of the foundations of such an approach and its applicability is needed. It is observed that the state-of-the-art in PHY-layer security methods have several limitations and challenges.

In this part of the project, we examine the principles of channel randomization and explore its application to achieve in-band message integrity and authentication. Especially, we focus on preventing active signal manipulation attacks and use reconfigurable antennas to systematically randomize the channel such that it is unpredictable to the active attacker. We developed a proactive and dynamical channel randomization approach to defend against active signal manipulation attacks in the wireless physical layer. We established a signal cancellation attack and defense framework to model the attacker's behavior. Based on the analytical results, we proposed a PHY- layer message integrity protection scheme which uses reconfigurable antennas for channel randomization. Comprehensive experiments were carried out to evaluate the proposed approach under different attack scenarios. Besides defending against signal manipulations, the proposed channel randomization method can also be used to enhance other PHY-layer security objectives, or defend against new attacks. For example, prevent cancellation of the jamming signal by multiple antenna attackers in friendly jamming, or known plain text and cipher text only attacks against artificial-noise based secret communication schemes, such as orthogonal blinding. For the latter, a key to successful attacks is the well- trained adaptive filters which filter out the artificial noise. However, the filter is trained over multiple symbol duration, during which the legitimate channel is static. Utilizing our proactive and dynamic channel randomization approach can defeat these attacks by preventing them from successfully training the filter.

A detailed analysis of the proposed schemes is available in [1].

3.1.2 Robust Physical Layer Security With MR-MIMO

In this part, we extend our efforts in physical layer security. We investigate the use of reconfigurable antennas to achieve robust physical layer security. Wireless channels are prone to wiretapping. Even though encryption techniques can be employed to protect the privacy of communication, once the signal is compromised, it is a matter of time to decrypt the signal. To prevent the reception of signals by unwanted receivers, physical layer security (PLS) techniques have been developed. In this work, we reformulate the PLS problem to arrive at a more robust technique that can not only boost the security of wireless signals but also maintain the data rates to intended users.

System Model

We consider a multi-user MIMO (MU-MIMO) wiretap channel between a legitimate transmitter employing M MRAs, and one or more legitimate receivers in the presence of one or more eavesdroppers. We assume all legitimate receivers employ MRA elements in their antennas while eavesdroppers are equipped with non-reconfigurable antennas. Let there exist L legitimate receivers with receiver-l employing N_l MRAs and K eavesdroppers with eavesdropper-k equipped with E_k antennas. We can express the revived signal at legitimate receiver-l as

$$\boldsymbol{r}_l = \boldsymbol{H}_l(\boldsymbol{\mu}, \boldsymbol{\nu}_l)\boldsymbol{P}\boldsymbol{s} + \boldsymbol{n}_l,\ l = 0, \ldots, L-1, \tag{1}$$

where $\boldsymbol{H}_l(\boldsymbol{\mu}, \boldsymbol{\nu}_l)$ is the $N_l \times M$ channel matrix between the transmitter and legitimate receiver-l, $\boldsymbol{P} = [\boldsymbol{P}_0 \ldots \boldsymbol{P}_{L-1}]$ is the composite precoder matrix with $\boldsymbol{P}_l$ denoting the precoder for receiver-l, and $\boldsymbol{s} = [\boldsymbol{s}_0^T \ldots \boldsymbol{s}_{L-1}^T]^T$ is the transmitted signal vector with $\boldsymbol{s}_l = [s_{l,0} \ldots s_{0,v_l-1}]^T$ denoting the transmitted signal for receiver-l. The received signal at the eavesdropper is given by

$$\boldsymbol{y}_k = \boldsymbol{G}_k(\boldsymbol{\mu})\boldsymbol{P}\boldsymbol{s} + \boldsymbol{n}_k,\ k = 0, \ldots, K-1, \tag{2}$$

In (1) and (2), the vectors $\boldsymbol{\mu} = [\mu_0 \ldots \mu_{M-1}]$ and $\boldsymbol{\nu}_l = [\nu_{l,0} \ldots \nu_{l,N_l-1}]$ denote the underlying MRA modes at the transmit and receive antennas of legitimate nodes. In the absence of eavesdroppers, the transmitter can select the MRA modes $\boldsymbol{\mu}$ and $\boldsymbol{\nu}_l$ to optimize the multi-user MIMO transmission to L users such that $\sum_{l=0}^{L-1} \leq M$. In the presence of eavesdropper, the transmitter also tries to minimize the data rate to those receivers. Here, we develop novel MRA mode selection and MRA design techniques that can achieves various trade-offs between maximizing the capacity between transmitter and legitimate receivers and the level of physical layer security.

In this study, we focus on managing two properties of an MRA

- polarization: By intentionally maximizing mismatching the polarization of transmitted signals with that of eavesdroppers while letting legitime receiver MRAs to minimizing the mismatch, the information rate to eavesdropper can be blocked significantly.
- radiation pattern: MRA array has enhanced beamforming capabilities that can provide enhanced multi-user MIMO transmission opportunities creating additional degrees of design to further suppress signal emission towards any unwanted directions.

Dynamic combination of polarization and radiation pattern configuration can both reshape and utilize the multi-path prorogation medium to facilitate reliable and secure wireless transmissions while maintaining the channel capacity to legitimate receivers.

We assume that the transmitter and the legitimate receivers have channel state information. We consider two cases in regard to available knowledge at the transmitter:

- Case 1: The transmitter has no knowledge on eavesdropper channel.
- Case 2: The transmitted has the direction of departure towards eavesdropper channels.

Spatial Multiplexing/Diversity Tradeoff

With MU-MIMO transmission, we can share the available degrees of freedom between the spatial multiplexing gain, e.g., ranks of the transmissions to legitimate receivers, and the diversity order. For example, depending on the multi-path medium, we can vary the rank of users by manipulating the transmission directions. This helps create flexible beamforming opportunities while trading off spatial multiplexing gains with physical layer security levels, e.g., minimizing the rate towards eavesdroppers.

MRA Mode Selection

Mode Hopping: Transmitter changes its mode of operation according to a sequence which is known only to legitimate receivers. The polarization and radiation pattern of each mode in the sequence is chosen to create a maximum mismatch to some fixed antenna polarization pattern. The sequence of MRA modes and the MRA properties of each hop's mode is selected to randomize the wireless channel matrices. At each hop, the transmitter decides on the ranks of each legitimate user, $0 \leq v_l \leq M$, such that at each hop, at most M layers are transmitted. Hence, the available degrees of freedom are allocated among the legitimate users and remaining degrees of freedom are used to minimize the rate to eavesdroppers.

Precoder Design: The precoder is designed in conjunction with the mode of individual MRAs. We develop a modified zero-forcing precoder that slightly changes the direction of transmissions to legitimate users while minimizing the radiated power in all directions other than those of legitimate users.

MRA Design for MIMO Wiretap Channels

In order to efficiently control the desired and eavesdropper channels, one needs to have multiple polarization states for a given spatial radiation pattern. In addition, having MRA modes that can create single or simultaneous multiple beams is also required to exploit spatial degrees of freedom. We employ Genetic Algorithm (GA) to design such MRA modes.

Simulation Analysis

A detailed analysis on the performance of MRA-based PLS and the design approaches are currently under preparation for submission to IEEE Transactions on Wireless Communications [2].

3.1.3 Online Machine Learning for MRA State Selection

In earlier work of this project, we have developed dynamic mode selection techniques. Those approaches have focused on a quasi-static channel conditions where the first or second order statistics of the channel remain the same. In practical channels where MRA would benefit the most, the channel statistics or states may vary and thus one would require the MRA mode switch to efficiently track and adopt to changes. In addition, by properly changing the operation mode of MRAs, we are creating the radiation pattern of the antenna which in return effects the channel realizations. In this part, we introduce the use of various online machine learning techniques to determine winning operational modes of the MRA array.

System Model

We consider an OFDM based SU-MIMO transmission where a transmitter with M MRAs wishes to send information to receiver with N MRAs. The multi-path medium is modelled using a 3D spatial channel model with K resolvable clusters where each cluster has B subpaths. For a given set of MRA modes, the spatial characteristics of the channel can be manipulated as desired. In this work, we investigate the

time variation of second-order statistics of the MIMO spatial channel with respect to antenna mode. We note that the multi-path medium may also undergo some unknown variations. Our goal in this part is to analyze the time-domain behaviour of the wireless channel and find suitable learning techniques to concurrently modify the MIMO channel to maximize the information capacity while allowing for reliable channel estimation. This problem is different from usual classification programs where we have an independent phenomenon creating different states to be learned. In the MRA mode selection problem, the selection of modes impacts the realized channel, so the learning process is inherently intervened with the design. It is seen that reinforcement learning techniques are suitable for this study.

Reinforcement Learning

Reinforcement learning is a reward based approach where a suitable selection of state is rewarded whenever such decision creates a preferred operation. The MRA mode selection for a SU-MIMO transmission suits well to this scenario. If a selected MRA mode creates a high-capacity wireless channel at a given situation, the algorithm stores the mode along with the underlying features of the channel. Here, the features are limited to covariance matrix of the channel.

Online Machine Learning

This type of machine learning is suitable for sequential learning where information is obtained in a temporal fashion. At each new set of data, one can update prediction on the upcoming states. In the MRA state selection problem, our objective is to determine new MRA states suitable for multi-path medium innovations. Since scatterers impacting the channel gains may vary over time, the set of MRA states need to be adopted to these variations. At the same time, one should be able to find a small set of MRA states to reduce the MRA selection complexity.

Selected OMLs for Investigation

We investigate two online learning methods: (i) recursive least squares and (ii) stochastic gradient methods. These are well known adaptive techniques that can efficiently predict the slowly varying conditions. For a given MRA state, the channel can be modeled as a stationary process. However, for different MRA states, the realized channel states may become less correlated. Here, we can establish a trade-off between learning performance and channel diversity. With increased channel diversity, which can be obtained by utilizing MRA states that can create channel states with low inter-state correlations, the system performance can be improved. The drawback is that, predicting such suitable MRA states become challenging since learning algorithm will not be able to benefit from temporally smoother variations.

In an effort to improve the learning quality and system diversity, we develop a group based multi-layer sequential learning where we determine MRA states that behave similarly (in terms of attained performance (channel capacity), channel covariance matrix, MIMO channel rank, etc.) against the multi-path fading channel. For each MRA state group, a training process is instantiated in which each MRA state is tracked separately and predicting the new MRA states that are not currently member of the underlaying MRA state group is made based on aggregate behaviour of the group. The aggregation provides more reliable metric in predicting a better future state.

The training of states start with a properly selected set of MRA sets that are grouped according to correlations among radiation patterns. The groups in this fashion are generated in an iterative manner where we mark an MRA state as a group header if its pattern correlation with any existing MRA group

header is lower than some predefined threshold. By twining the correlation threshold, we can adjust the number of groups and number of states in any MRA group. Once the MRA groups are initialized, MRA states other than group headers in each group are sorted in a descending order according to pattern correlations. The groups are also sorted according to descending pattern correlations of the MRA group headers. This ordering is used in starting the initial training of MRA groups and MRA states within the groups.

While pattern correlations establish a measurable relation among the corresponding realized channel states, the multi-path scatters can create decorrelation among channels even for similar MRA states since the final channel is a complicated superposition of various rays created by a mixture of different polarized EM waves' propagations. This calls for on-line training of MRA states to determine suitable states. To that end, we develop an efficient training and prediction procedure.

- Initial training: MRA group headers are employed first for initial training subsequently. This initial procedure allows to collect the correlation information among the MRA groups. Since a single MRA state may not contain sufficient information for a given group, we train the second MRA states in each group (if available), and store the realized channel correlation information. We train all available MRA states in this initial training procedure. We note that this exhaustive search over all states is performed rarely (e.g., minutes, hours or even days depending on the wireless system's spatial variational characteristics). Based on resulting realized channel states and relative correlation with respect to the header state of MRA group-0. The pattern correlation and observed channel correlation information are employed to adjust the MRA groups.
- MRA group update: Afet collecting the correlation information from initial training, we next start updating the group states. If within an MRA group, the product of normalized channel correlation of a state with the group-header is lower than some predefined threshold, then that MRA state is removed from the group and marked as a new group header. All MRA groups are updated accordingly. At the end of group updates, we may end up with reduced groups and new MRA group headers.
- Periodic training: Followed by MRA group update, MRA groups are continued to be trained periodically.

We note that data transmission continue along with MRA state training, that is, training of the MRA states are performed on a small subset of sub-carriers in the OFDM symbol. Since the periodic training is performed group-wise, the impact on data transmission is minimized during the sequence of MRA-group training. Switching from one group to another may have some limited impact. If an MRA group is not providing desirable performance during training, it is dropped from periodic training until the MRA groups being actively employed during periodic training starts to fail data transmissions. In this regard, we use least-squares and stochastic gradient approach to calculate the performance variation (capacity, or channel correlation matrices). During the coarse of periodic training, the classification algorithm will continuously update MRA groups and MRA group members based on the gradients by the underlying sequential learning algorithm.

Simulation Study

We are currently analysing the performance of OML based MRA state prediction over spatial MIMO channel model that can statically predict the behaviour a typical propagation set-up. The results will be reported in the journal paper [3].

3.1.4 Fast Calibration of MRA Arrays

A major drawback for antenna array systems is the potential irregularities and non ideal conditions impacting RF, antenna and the feed circuitries. In order to attain the offered gains, RF paths and antenna arrays need to be calibrated so that the final beam shapes are created as desired. MRA arrays contain both array and element related in accuracies. In order to benefit directional features of MRA array, both element and array level calibrations are required. Due to many available states, we need efficient methods to calibrate MRA array. We develop MRA mode subset selection methods to calibrate the array so that one would not need to calibrate for all modes of operation.

System Model

Let us consider a generic MIMO communication system with M transmit MRAs and N receive antennas. Let $x_m(f,\mu) = e^{j\angle\phi_m(f,\boldsymbol{\mu})}$ denote the unknown phase rotation for RF branch m connected to MRA-m at state-$\boldsymbol{\mu} = [\mu_1 \dots \mu_M]$, and frequency-$f$. Here, we investigate a simplified RF path error model where a frequency and antenna independent time-delay from digital unit to antenna tip is present along with a fixed but unknown phase bias that is dependant on the MRA mode:

$$\phi_m(f,\mu_m) = 2\pi f t_m + \phi_m(\boldsymbol{\mu}) \tag{3}$$

For a complex input signal $\boldsymbol{s} = [s_1 \dots s_M]^T$, we can express the signal at MRA elements as

$$\boldsymbol{y}(f,\boldsymbol{\mu}) = \boldsymbol{X}(f,\boldsymbol{\mu})\boldsymbol{s} \tag{4}$$

with

$$\boldsymbol{X} = \text{diag}(x_1(f,\boldsymbol{\mu}),\dots,x_M(f,\boldsymbol{\mu})).$$

The signals at MRA-m, $m = 1,\dots,M$, are captured by a coupling circuitry per MRA element and provided as a feedback to the digital unit where the signals are processed to estimate the RF-path errors and determine compensation weights for each RF branch.

We note that each MRA mode state $\boldsymbol{\mu}$ may result in a different phase error. With M antennas and L states per MRA element, we have M^L different states for the MRA array. In case of large M and L values, calibration of the array becomes prohibitive if each and every state of the array is attempted to be calibrated. On the other hand, by judiciously selecting of MRA states for calibration, it is possible to calibrate a smaller set of MRA states and predict the calibration required for other states.

Hierarchical Calibration with OFDM signalling

Observing that M^L states can easily become prohibitive for even small MRA arrays, we investigate the opportunities of reducing the complexity. To that end, it is seen that the calibration of parasitic layer and the patch layer can be treated separately under certain approximations. For example, the impact of mutual coupling over MRA elements can be ignored with respect to the calibration errors existing in the RF-antenna feed circuitries. Since RF-antenna feed lines are dominant sources of calibration errors, the process of calibrating RF-lines can be performed independently from MRA element calibration. In addition, using OFDM transmission, we can modulate each MRA element with an orthogonal subcarrier and thus, perform element calibration in parallel. In addition, observing that phase offset of MRA's parasitic layer is almost frequency independent as opposed to the RF line's phase offset (due to timing error as seen above in (3)), we can set different MRA states at each element of the array. These observations allows us to calibrate a large number of MRA states in a shorter period. However, one

would still need to perform multiple observations per MRA state to get an accurate offset estimation. In the presence of a larger number of MRA states, the overhead of training may still be large.

Selection of Calibration States

In order to further reduce calibration training overhead, let us closely investigate an individual MRA element in the array. Similar parasitic layer geometries are expected to create similar phase offsets in the RF feed network. If a parasitic layer geometry resulting from a given state can be expressed as an axial rotation of a parasitic layer for another MRA state (rotation around the axis perpendicular to array plane), the resulting radiation pattern is also expected to be a rotated version of that MRA state. So, during the calibration, MRA states having similar array geometries can be merged in to subsets of modes. In this work, we focus on 2D rectangular uniform arrays with rectangular parasitic layers. Thus, there exist several states that can be grouped into same subset for calibration purposes.

For example, consider a 3×3 rectangular parasitic layer with 12 switches (see Fig. 1). Due to axial symmetry (this example is almost a square parasitic layer of identical square metallic pixels), many of the states create similar parasitic geometries. For example, the case of switching one of the outer switches (e.g., PINs 1, 2, 4, 6, 7, 9, 11, 12) to ON state while setting all others to an OFF state can be viewed same state for calibration purposes since the parasitic layer can be obtained by rotating around the broad-sight axis; thus, this reduces 8 states into a single-state. Similarly, we can find several other states that can create rotationally similar parasitic geometries. After determining the calibration similarity groups, we can calibrate one of the members of the group and use the calibration offset for the group. In order to have a robust calibration, we can train the calibrated states within a group in a round-robin fashion over time (e.g., different calibration instances) and hence remove any residual difference in between the MRA states in the same subset.

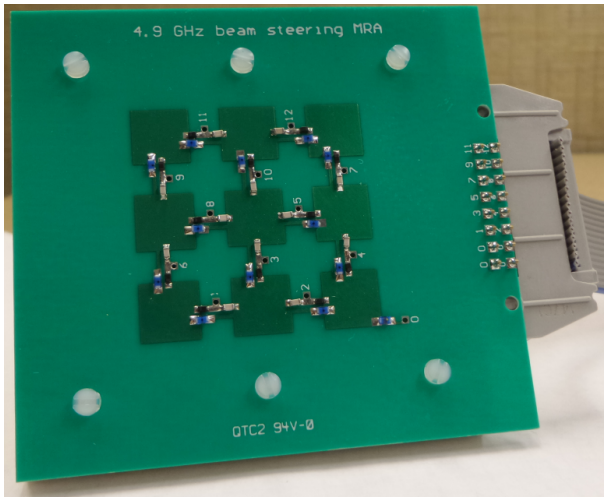

Figure 1: The upper face of the fabricated parasitic layer with switch numbering and integrated SMD components.

Sequential Estimation

We employ a recursive least squares (RLS) estimation type method to solve for the filter weights that minimize the calibration error between the signals received by the coupler and the transmitted pilot sequence. Different from legacy non-reconfigurable arrays, we can set different MRA states per RF-antenna line. For each MRA state per element (in case of calibration subset generation, one MRA state

per group), we maintain a separate RLS estimator. To reduce the estimation error, we can train each MRA element for a pre-specified times and perform a windowing average.

Simulation Analysis

The results of this work is currently under preparation for submission to IEEE Trans. on. Antennas and Prorogation [4].

3.1.5 Hybrid Precoding for Massive MRA Arrays

We have continued our investigations on hybrid precoding technique for massive MRA array. Recall from the previous years report that this approach allows us to reduce the complexity of MRA array design without sacrificing attainable performance from massive arrays. In addition to analyzing the performance of proposed techniques on typical 5G systems, we have also extended our approaches to to determine optimal array geometries suitable for underlying multi-path medium and spatial receiver distribution.

Planar MRA Array and Hybrid Precoding

For a $N_v \times N_h$ uniform planar array of $N = N_v N_h$ MRA elements, let there exist N_g RF chains with both amplitude and phase control, and let us assume each RF chain is connected to N/N_g phase shifter circuitry feeding each of which driving a single MRA element. We assume that the digital baseband part provides an $\boldsymbol{x} = N_g \times 1$ signal vector to RF chain with amplitude/phase gain. The received signal can be expressed as

$$\boldsymbol{r} = \boldsymbol{H}(\boldsymbol{\mu})\boldsymbol{W}\boldsymbol{A}\boldsymbol{P}\boldsymbol{s} + \boldsymbol{n} \tag{5}$$

where we have the following parameters:

- $\boldsymbol{s}$ is a $L \times 1$ signal vector with $\boldsymbol{P}$ denoting the $N_g \times L$ digital precoder matrix where we can express the signal to RF chains as
$$\boldsymbol{x} = \boldsymbol{P}\boldsymbol{s}$$
- $\boldsymbol{A} = \text{diag}(\alpha_0, \ldots, \alpha_{N_g-1})$ is the analog beamforming matrix with amplitude and phase modulation,
- $\boldsymbol{W}$ is the $N \times N_g$ matrix describing the phase shifter connections from N_g RF branches to N/N_g MRA elements. Note that each column of $\boldsymbol{W}$ has exactly N/N_g unit-magnitude complex gains and all other terms in the column is 0.

Note that the design of $\boldsymbol{W}$ plays an important role since it defines the sub-array geometry that can be optimized to create the desired beam patterns. For example, for a zero-phase shift where RF-branch-k, $k = 0, \ldots, N_g - 1$ is connected to MRA-$kN/N_g + n$, $n = 0, \ldots, N/N_g - 1$, we have

$$\boldsymbol{W} = I_{N_g} \otimes \mathbf{1}_{N/N_g \times 1} \tag{6}$$

Combination of available precoders, $\boldsymbol{P}$, and analog processing capabilities of $\boldsymbol{A}$ and $\boldsymbol{W}$ creates a rich set of design space allowing for attaining vastly different coverage shapes. In conjunction with the MRA elements configuration, tremendous flexibility is achieved. The design of $\boldsymbol{W}\boldsymbol{A}\boldsymbol{P}$ along with MRA state design is not trivial as expected. In this work, we resort to a number of simplifications to grasp the available performance improvement opportunities:

- We assume a code-book based precoding where $\boldsymbol{P}$ are selected among DFT beams, e.g., digital beam scanning,
- Identical MRA states is a activated in any realization of the array,
- We can express $N_g = N_{g,v}N_{g,h}$, and N_v and N_h as integer multiples of $N_{g,v}$ and $N_{g,h}$ respectively.
- Analog phase shifter connections are allowed to create identical subarray geometries for each RF line with amplitude/phase control.

These assumptions let us evaluate the radiation pattern of any realized element using the principle of pattern multiplication. With this formulation, we can model different forms of arrays of subarrays (e.g., uniform 2D or interleaved array) that can be optimized to attain desired coverage profile. Since the design is a highly non-convex and a combinatorially complex problem, we can resort to heuristics based search techniques such as Genetic Algorithm. To that end, let as assume the 3D desired coverage shape is given by $R(\theta, \phi)$. The goal is the determine the set of $\boldsymbol{W}$ to achieve the largest beam forming gain profile and closest to target $R(\theta, \phi)$. Let us express the final beamformer as

$$\boldsymbol{U} = \boldsymbol{W}\boldsymbol{A}\boldsymbol{P} \tag{7}$$

where $\boldsymbol{U} = [\boldsymbol{u}_0 \dots \boldsymbol{u}_{L-1}]$ with $\boldsymbol{u}_l$ denoting the lth beamformer, $l = 0, \dots, L-1$. The digital precoders are selected such that each layer is beamformed via a DFT vector. We can define the beam-pattern profile as the envelope of all layers' radiation pattern for each DFT assuming a fixed $\boldsymbol{A}$ and $\boldsymbol{W}$. Then by optimizing the analog beamforming components to attain the closes beam pattern to target beam pattern. By repeating this search for each available MRA state, we can determine the preferred MRA-modes t achieve the optimum beam-pattern profile.

$$\boldsymbol{\mu}^* = \arg \min_{\boldsymbol{\mu}, \boldsymbol{A}, \boldsymbol{W}, \boldsymbol{P} \in \mathcal{P}} E\{\|f(\theta, \phi) - R(\theta, \phi)\|^2\} \tag{8}$$

where $\sum_{r=0}^{N-1} |u_{l,r}| = N/N_g$ and $f(\theta, \phi) = |\boldsymbol{u}_l^H \boldsymbol{a}(\theta, \phi) E(\theta, \phi|\mu)|^2$ is the radiation pattern of the hybrid array. During the optimization, we quantize the analog phases (for all analog lines) and amplitudes (for the N_g RF branches) and limit the $\boldsymbol{W}$ to those resulting in either a non-interleaved 2D uniform array, or interleaved uniform arrays.

Using the Genetic Algorithm with multi-objective optimization, we obtain several pareto-optimal solutions with preferred MRA states that can attain the target coverage shape. Two journals are currently under preparation to provide extensive analysis on the proposed hybrid MRA array techniques [5, 6].

3.2 MRA and MRAA Design and Fabrication

3.2.1 High-gain MRA Design

A broadband and high gain antenna, which operates at (3.2-4.2) GHz band and achieves maximum $\sim$12.3 dB realized gain, has been presented. The antenna architecture consists of a driven aperture coupled stacked patch antenna on top of which parasitic radiators are placed. A prototype antenna has been fabricated and characterized. The main advantage of the presented antenna is its high gain which is maintained over a wide bandwidth. This property is very important to improve the signal to noise ratio (SNR) of point to point communication systems.

Introduction

Low profile, ease of integration with monolithic microwave integrated circuits (MMIC), fabrication in standard printed circuit board (PCB) processes, light weight and low cost have made patch antennas attractive for various types of communication systems. However, narrow bandwidth ($2-3\%$) and low gain ($\sim$5dB) makes patch antennas impractical for many applications, e.g. point to point communications. Numerous techniques have been proposed to improve the gain and bandwidth of the patch antennas [7, 8]. While thicker and low permittivity substrate or wide-band matching networks can be used to increase the bandwidth, problems associated with surface waves and design complexity makes them impractical [7]. Stacked patch configuration, where a driven patch is mutually coupled to a parasitic patch placed on top of it, offers a simple solution for improving patch antenna impedance bandwidth [9]. In this configuration, driven patch and closely located parasitic patch produces two near-resonant frequencies which combines to give a broad bandwidth.

Providing relatively constant high gain over broad bandwidth is crucial for obtaining high signal to noise ratio (SNR) in long distance communication. Partially reflective surface [10], rectangular loop shaped parasitic radiator [8], leaky resonator [11], substrate-superstrate resonance [12] and engineered magnetic superstrates [13] are some of the proposed techniques for obtaining high gain. While these techniques offer significant gain improvement over the standard patch, they provide gain improvement over a small bandwidth and some of them result in a bulky structure. Metasurface, which is a two-dimensional planar surface composed of electrically small metallic scatterers, has been used to improve gain of the patch antenna [14, 15]. These metasurfaces with near-zero permeability and negative surface magnetic susceptibility provides a cost-effective and compact solution for increasing antenna gain. In addition, passive/parasitic radiators, which are placed in the vicinity of the driven antenna, can also be used to enhance the directive gain of driven antennas [16, 17]. These passive radiators parasitically absorbs EM waves from the driven antenna and reradiates them. When the reradiated waves are in phase with the incident waves, they add constructively and enhances the directive gain.

In this work, stacked patch with a novel three layer parasitic structure, consisting of a reflective metasurface and two metallic strip passive radiator, has been designed to provide high bore-side gain over the broad bandwidth. This antenna provides a simple and low cost solution for commercial applications requiring high gain over a broad bandwidth.

Antenna Structure

The geometry of the antenna with critical dimensions is shown in Fig. 2. The presented antenna consists of 5 layers, namely driven antenna, stacked patch and 3 parasitic layers. Driven antenna is an aperture coupled patch antenna, where a microstrip line with 50Ω characteristic impedance feeds the radiating patch($18mm \times 18mm$) through an aperture($16mm \times 0.8mm$) located under the center of the patch in the metal ground plane. A stacked patch($22mm \times 22mm$), which is slightly larger than the driven patch, is placed above the driven patch. The distance between the driven patch and stacked patch has been numerically optimized to obtain the maximum possible bandwidth. Feed, driven patch and stacked patch metalizations are formed on R04003C ($\epsilon_o = 3.55, \delta = .0027$)substrate with 0.8, 3 and 1.5 mm thicknesses, respectively. Three parasitic radiators (indicated as parasitic layers-1,2,3 in Fig. 2) have been placed on top of the driven antenna. Parasitic layer-1 consists of 7×7 grid of corner connected metallic ring, which act as a metasurface. Parasitic layers-2 and 3 consist of two passive metallic radiators. The dimensions of metasurface and the two passive radiators are optimized using a full-wave simulation tool (i.e. Ansys HFSS [18]) to obtain a relatively flat gain over the whole frequency band.

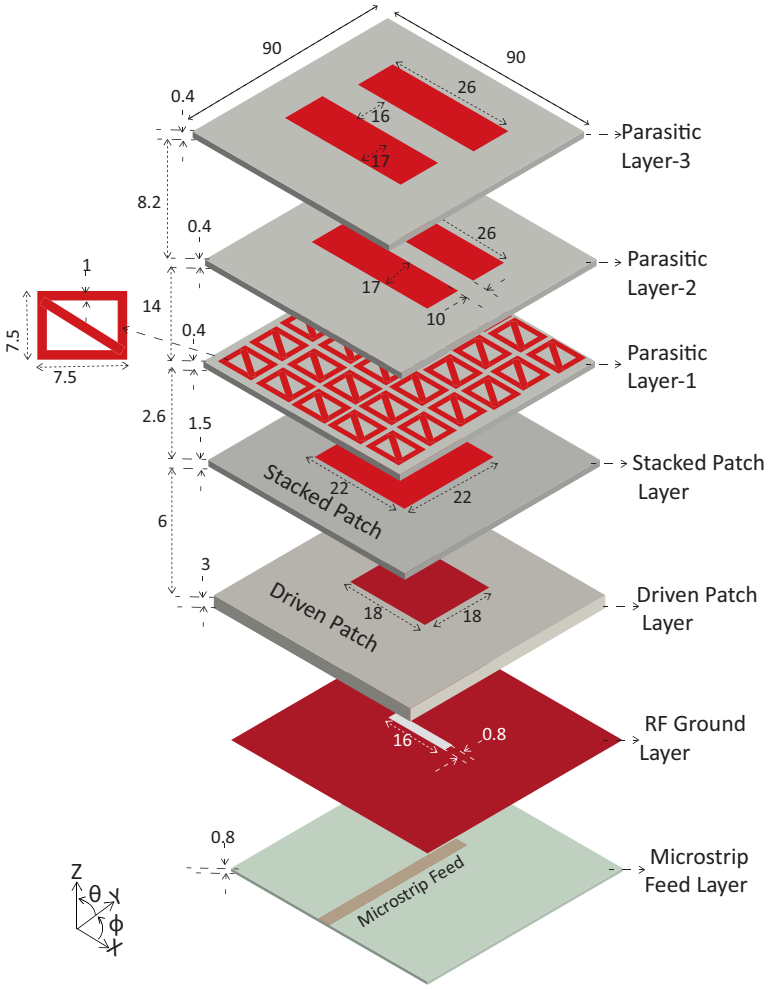

Figure 2: 3D perspective view of the antenna[all dimensions are in mm]

Measurement And Simulation Results

A prototype antenna was fabricated using standard PCB fabrication processes. Impedance performance of the antenna was characterized using a vector network analyzer (VNA) to validate the simulation results. Simulated and measured reflection coefficients are shown in Fig. 3(a) indicating a good agreement between them. It can be observed from Fig. 3(a) that the antenna covers (3.2-4.2) GHz band. To show the impact of the parasitic layers on gain enhancement, the simulated realized gains of the antenna with and without parasitic layers with respect to frequency are shown in Fig. 3(b). The antenna with parasitic layers achieves as large as 4 dB more realized gain compared to the antenna without the parasitic layers. Also notice that the presented antenna has relatively constant realized gain over the whole frequency band (3.2-4.2)GHz. Realized gain patterns at 3.2 and 4 GHz are shown in Figs. 3(c) and (d) respectively, which indicates that the antenna retains the integrity of the radiation pattern across the whole band.

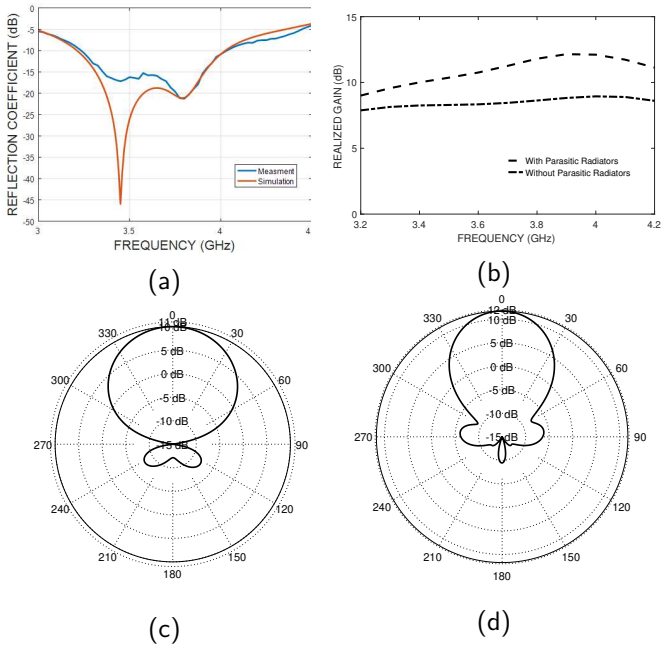

Figure 3: (a)Simulated and measured reflection coefficients, Simulated (b) realized gain vs frequency, (c) realized gain pattern in Y-Z plane at 3.2 GHz, and (d) realized gain pattern in Y-Z plane at 3.6 GHz,

Conclusion

A novel parasitic radiator structure in conjunction with well-known stacked patch antenna configuration have been used to obtain high gain which stays relatively constant over a broad bandwidth (3.2-4.2)GHz. Reflection coefficient of the fabricated prototype indicated close agreement between simulation and measurements. Simulated realized gain with respect to frequency and realized gain patterns at two different frequency points indicated that the realized gain remain relatively flat with pattern integrity retained over the entire bandwidth of (3.2-4.2)GHz.

3.2.2 MRA Optimization For Non-ideal Conditions

In this section, we present the error vector magnitude (EVM), intermodulation (IM) and radiation performances of a reconfigurable antenna (RA) capable of varying its bandwidth between 3.4-3.6 GHz and

3.1-3.9 GHz bands, and steering its main beam into three directions pertaining to $\theta \in \{-30^\circ, 0^\circ, 30^\circ\}$, $\phi \in \{0^\circ\}$ for each band. Two parasitically coupled reconfigurable layers located on top of a driven antenna used in conjunction with a reconfigurable feed layer employing PIN diode switches enable concurrent configuration of impedance bandwidth and radiation pattern. Maximum realized gain of $\sim$9 dB has been achieved for all modes of operation as shown by measurements and simulations. Measurements indicated less than -25dB (5.6%) EVM for input powers up to 30dBm and revealed that the combined effects of loose solder joints and large non-linear response of PIN diodes are the main factors resulting in passive IM products.

The multi-layer RA based on reconfigurable parasitic layer technique presented in this work is capable of performing both wide and narrow bandwidth operations while at the same time providing beam steering towards three different directions. Achieving concurrent bandwidth and pattern reconfigurability in a single compact platform is novel in that it provides advantages in effective sensing, transmission and frequency reuse [19–21].

Reflection coefficient and radiation pattern are most commonly used to characterize antennas. To determine the benefits of RAs used in a transceiver system requires characterizing the impacts that an RA plays on error vector magnitude(EVM) used as measure to quantify the performance of a transceiver. Also, signal distortion due to intermodulation (IM) products, whether it is passive IM (PIM) or is due to active elements, such as PIN diodes used in an RA, need to be measured. Although for traditional non-reconfigurable antennas some works investigated EVM [22, 23] and passive intermodulation (PIM) [24, 25], this has not been done for RAs. To that end, this work puts a great deal of efforts on characterizing the IM and EVM performances of the proposed RA. The main novelty of the presented RA is its capability to achieve simultaneous configuration of impedance bandwidth and radiation pattern by jointly using three reconfigurable layers, which are reconfigurable patch, pixel and feed layers as explained in the next section. Maintaining a high realized gain ($\sim$9dB) for all modes over the whole operational bandwidth is another important property achieved by this compact RA structure.

Antenna Structure and Radiation Characterization

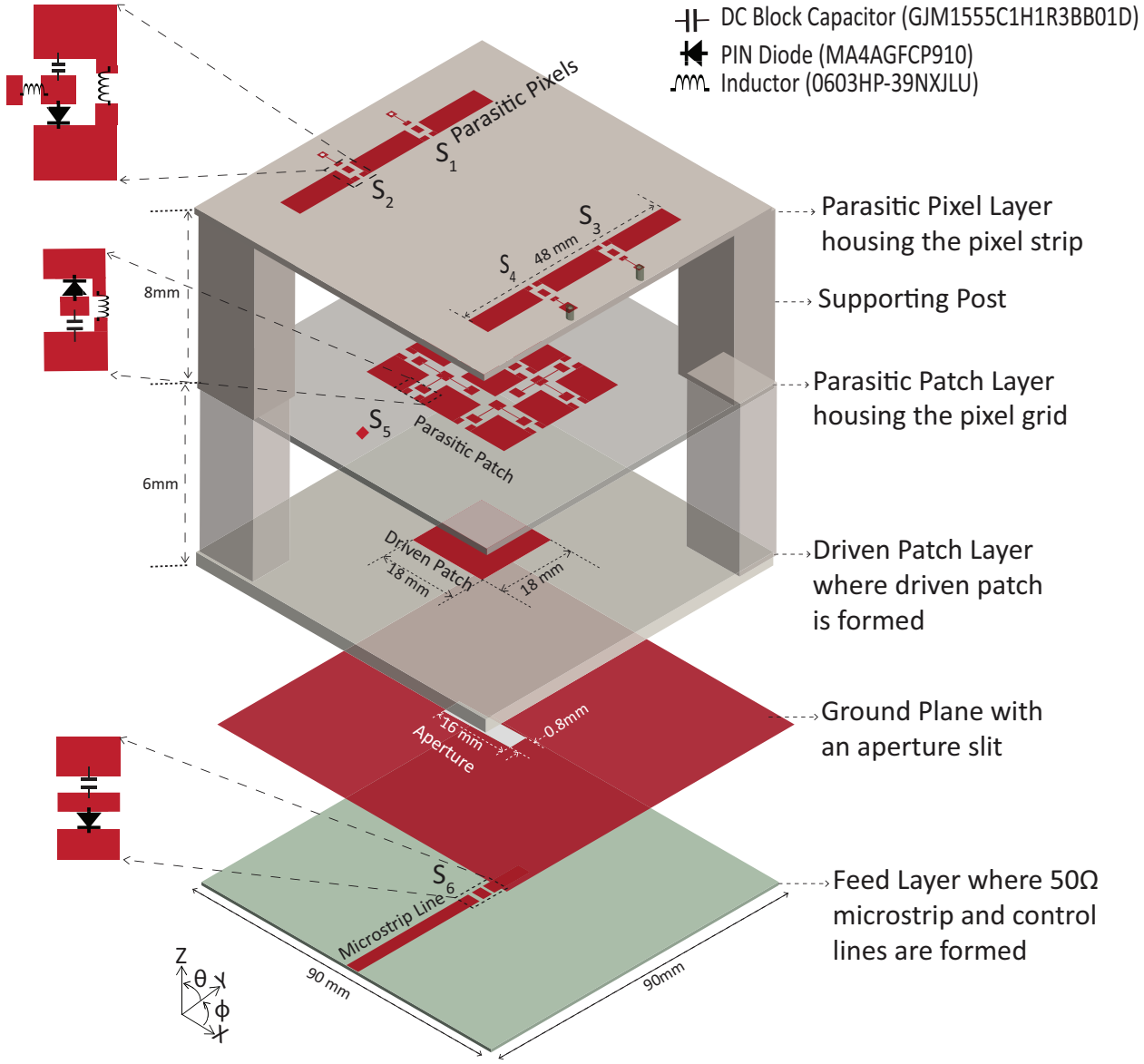

Figure 4: 3D exploded view of the RA

The geometry of the RA and pixels interconnected by PIN diodes are shown in Fig. 4. The structure consists of four main layers, namely feed, driven antenna, parasitic patch and parasitic pixel layers. The working mechanism of this RA is based on well-established reconfigurable parasitic layer approach [26]. By connecting and disconnecting, the grid of 3×3 and 3×2 metallic pixels placed on the upper surfaces of the parasitic patch and pixel layers, respectively, and also controlling single PIN diode inserted in the microstrip feed line enables to achieve the reconfigurable modes of operations in terms of bandwidth and beam direction. The switches' status and corresponding modes are given in Table 1.

A prototype RA was fabricated using standard printed circuit board fabrication processes and measured.

Table 1: Switch Configurations and associated modes

Modes	θ	ϕ	BW(MHz)	S_1	S_2	S_3	S_4	S_5	S_6
1	0^o	0^o	200	0	0	0	0	0	1
2	30^o	0^o	200	0	0	1	1	0	1
3	-30^o	0^o	200	1	1	0	0	0	1
4	0^o	0^o	800	0	0	0	0	1	0
5	30^o	0^o	800	0	0	1	1	1	0
6	-30^o	0^o	800	1	1	0	0	1	0
11	N/A	N/A	N/A	0	0	0	0	0	0
22	N/A	N/A	N/A	0	0	1	1	0	0
33	N/A	N/A	N/A	1	1	0	0	0	0

PIN diode switches are numbered in Fig.4 as $S_i(i = 1 \ldots 6)$, where $S_i(i = 1,2,3,4)$ are the switches integrated on parasitic pixel layer, S_5 represents the twelve switches used in parasitic patch layer, and S_6 is the switch integrated on microstrip feed line. The simulated and measured reflection coefficients and realized gain patterns for modes 1-6 are shown in Fig. 5 with good agreement between simulations and measurements. As predicted by simulations, the measured results show that modes 1,2 & 3 and modes 4,5 & 6 correspond to narrowband (3.4-3.6 GHz) and broadband (3.1-3.9 GHz) operations, respectively. The maximum realized gain is ∼9dB for all modes.

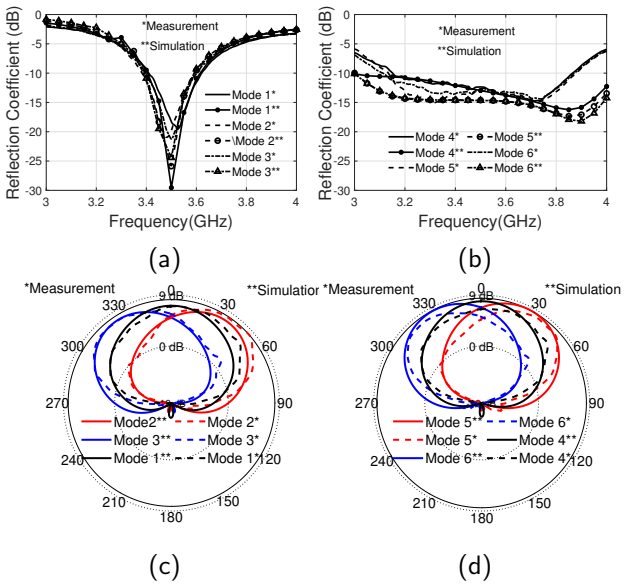

Figure 5: Simulated and measured reflection coefficients of the RA for (a) mode 1,2, 3, (b) modes 4,5,6 and realized gain patterns at 3.5 GHz for (c) modes 1,2,3, and (d) modes 4,5,6

EVM and PIM Characterization

EVM Characterization

EVM is commonly used to quantify the performance of a transceiver system, where the relative positions of the constellation points of an ideal case and non-ideal case considering non-ideal factors, are measured and compared. To determine the impact that the presented RA plays on EVM, a measurement set-

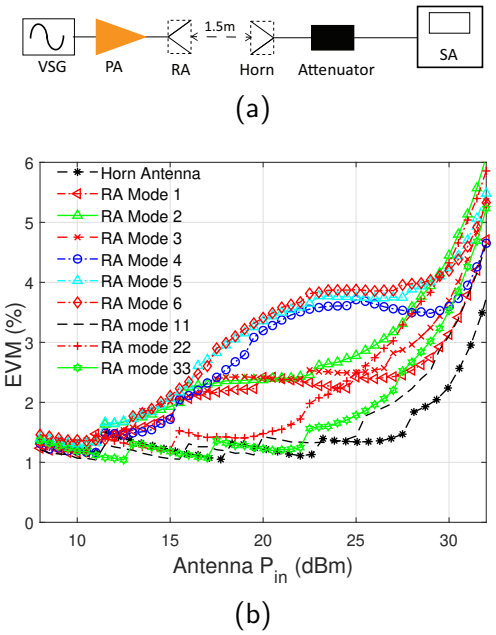

Figure 6: (a) Schematic of the AUT measurement set-up and (b) measured EVM results for the RA modes and horn antenna, & extra RA modes (modes 11,22 &33) as a function of input power P_{in}

up consisting of a vector signal generator (VSG) [27] and spectrum analyzer (SA) [28], as shown in Fig. 6(a) is used. In this set-up, VSG is used as a transmitter, where a quadrature amplitude modulation (QAM)-64 signal in the desired 3.5 GHz band is generated and is received by the SA. Only one modulation scheme is used as modulation scheme has little impact on EVM in either high or low distortion environment [29]. Before characterizing the EVM performance of the RA, the measurement setup was validated by performing two preliminary tests. In the first test, the VSG was directly connected to the SA, and EVM was measured as a function of input power (P_{in}). It was observed that the measured EVM is below -37dB (1.4%) for the range of P_{in}, -25dBm$< P_{in} <$0dBm. The degradation of the EVM corresponding to P_{in} <-25dBm is due to the reduction of signal to noise ratio (SNR), and for P_{in} >0dBm, there is a compression caused by the SA. Therefore, the measurement set-up was adjusted to provide the range of P_{in} values, -25dBm$< P_{in} <$0dBm, into the SA, which results in a 25dB measurement range and -37dB floor level. The second preliminary test was performed to assess the effect of the power amplifier (PA) [30] that was used in the RA measurements. The result revealed that the PA does not have a significant impact in the degradation of the EVM for output powers (P_{out}) <25dBm. However, the non-linearities of the PA introduce a degradation for P_{out} >25dBm reducing the measurement range to 20dB for EVM <-37 dB.

As a reference, the EVM of a passive ridge-horn antenna was first measured, which also served to verify the setup. Measured results for different modes of the RA and for the horn are shown in Fig. 6(b). Some degradation in EVM corresponding to RA modes as compared to the EVM of the passive horn was observed. This degradation is due to the use of the PIN diode switches in RA.

The EVMs corresponding to the modes 4, 5, and 6, and to the modes 1, 2, and 3 exhibit similar behaviors, where the EVMs of modes 4, 5, and 6 are degraded slightly more than those of modes 1, 2, and 3. As shown in Table 1, for modes 5 and 6, there are fourteen switches in ON state, with two being on the parasitic pixel layer and twelve being on the parasitic patch layer. For mode 4, there are twelve switches, which are all on the parasitic patch layer, in ON state. The EVMs of modes 5 and 6 are

almost identical, where the EVM of mode 4 is slightly better. These results indicate that the impact of the two switches on the parasitic pixel layer is less as compared to the impact of the PIN diodes on the parasitic patch layer. The impact of the switches of patch layer being more is due to two main factors: (1) larger number of switches, i.e., twelve vs. four, and (2) the closer proximity of the parasitic patch layer with the driven patch layer. For modes 2 and 3, there are three switches (two on the parasitic pixel layer and one on the microstrip feed line) in ON state, while for mode 1, there is only one switch (on the microstrip feed line) in ON state. The EVM of mode 1 is slightly better than those of modes 2 and 3. These results also indicate that the impact of the switches of parasitic pixel layer is relatively less. However, the impact of the single switch on the microstrip feed line (S_6) is possibly larger than those of the parasitic pixel layer switches. To further investigate the impact of S_6, the EVMs of three additional modes have been measured. These modes and their corresponding switch statuses are given in Table 1. Notice that these additional modes (modes 11, 22, and 33) have the same switch status with the modes 1, 2, and 3, except that S_6 is in OFF state. As seen from Fig. 6(b), the EVMs of modes 11, 22, and 33 are very close to that of a passive horn antenna. These results further indicate that the single switch on microstrip (S_6) plays a substantially larger role on the EVM performance than those of the four switches on the parasitic pixel layer.

The EVM characterization of the RA has revealed that the switch location in an RA architecture is as critical as the number of switches used. The impact of the interconnecting switch is increased when it is integrated into a region with increased RF signal strength. This is the case for S_6 integrated on the microstrip feed line. This also shows that the parasitic layer approach in RA design is an effective method as the degradation in EVM due to the switches integrated into parasitic pixel layer is negligible. It is worth noting that for $P_{in} >$ 25dBm, the EVM measurements show the combined effect of the PA and the RA. Despite some degradation, for all six modes of operations, the EVM of the RA is less than -25dB (5.6%) for $P_{in} \leq$30dBm, which is a good reference level for device validation purposes.

IM Characterization

Intermodulation (IM) products are generated due to the presence of nonlinearity, when a two-tone input signal of two closely spaced carriers at frequencies f_1 and f_2 feeds the antenna. The nonlinearity is either due to the use of nonlinear components such as PIN diodes or passive factors such as oxide layers that may exist between metal-to-metal contacts, electro-thermal effects, poor solder joints, and the use of ferromagnetic materials, i.e., nickel and steel. If IM products are located in the frequency band of interest, they cause interference with the desired signal resulting in distortion, which reduces receiver sensitivity. Also, it is worth noting that non-linear PIN diodes even unpowered or reverse biased and in the absence of PIM effects, may cause considerable non-linear distortions [31–33].

The IM characteristics of the presented RA were measured by using the set-up shown in Fig. 7. Two synthesizers [27] are used as sources to generate two carrier tones, where each individual tone is then amplified by a PA [30]. An isolator [34] is connected at the output of each PA to isolate them from the changes in the amplifier load conditions. The amplified carriers are combined by a combiner [35] and then fed to the RA through a directional coupler [36]. The directional coupler captures the signals reflected by the RA and channels them to SA [28], where the IM products are measured. A 20 dB attenuator is placed on the signal path going from the directional coupler to the spectrum analyzer so that the SA works within the adjusted optimum input power range (-25 dBm $< P_{in} <$ 0 dBm).

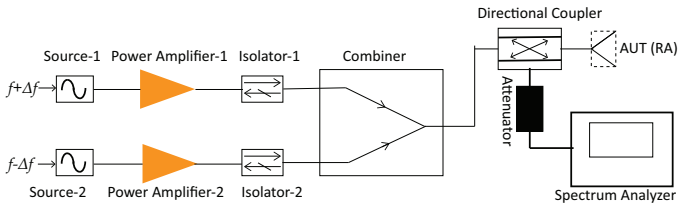

Figure 7: PIM measurement setup

The sensitivity of the measurements, which is determined by the measurable lowest power value of the IM product, is limited by two factors. One is the noise floor of the SA, which depends on its noise figure and the resolution bandwidth of the measurement, which can be as low as 10 Hz. The second limiting factor is the IM product generation by the internal mixer of the SA itself. From the specifications of the SA [37], where the optimum incident power on the mixer (-35 dBm for 10 Hz resolution bandwidth) and the dynamic range (95 dB) are given, the sensitivity of our measurements is -130dBm.

At first, the measurement set-up has been calibrated at 3.5 GHz in terms of RF losses and power readings of the spectrum analyzer. To this end, the output powers of the synthesizers have been calibrated so that the individual signal power at carrier frequency incident on the RA is adjusted to 30 dBm. The source-1 and source-2 are set at 3.5GHz+$\frac{\triangle f}{2}$ and 3.5GHz-$\frac{\triangle f}{2}$, respectively, while the IM product is measured for the band, $3.5GHz - 1.5\triangle f \leqslant f \leqslant 3.5GHz + 1.5\triangle f$. The measured PIM revealed that the actual sensitivity of the measurement set-up is $\sim$-110 dBm. Fig. 8 shows the measured IM power in dBc (relative to carrier power) as a function of $\triangle f$ for different modes of the RA. The IM performance of a legacy patch antenna, which is obtained by removing the parasitic layers and the single PIN diode on microstrip feed line (S_6) of the RA, was also measured and used as a reference. All the RA modes show relatively high IM power compared to the legacy patch antenna, which is expected due to the use of substantial number of switches in the multilayer RA.

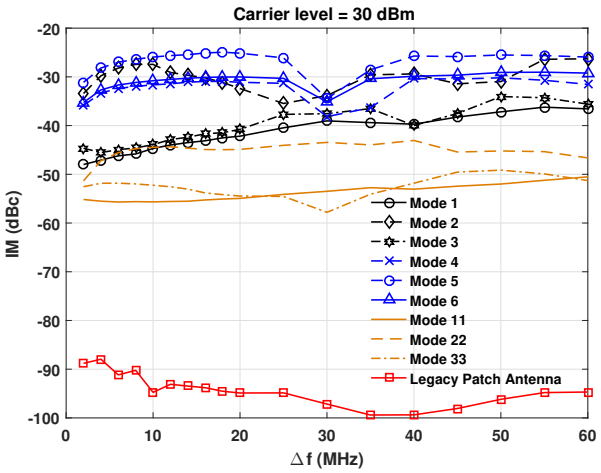

Figure 8: PIM measurement results of the RA

Modes 4, 5 and 6 show the largest degradation in IM performance. While modes 4 and 6 show very similar behaviors with mode 4 performing slightly better, mode 5 has relatively higher IM power. As seen in Table 1, these modes have the largest number of switches in ON state, where mode 4 uses twelve

ON-state switches (all on parasitic patch layer), modes 5 and 6 use fourteen ON-state switches (two on parasitic pixel layer and twelve on parasitic patch layer). The small degradation in IM performance of mode 6 as compared to mode 4 is as expected and can be attributed to the two ON state switches of parasitic pixel layer (S_1 and S_2). Mode 5 for which the other two parasitic pixel layer switches (S_3 and S_4) are in ON state, exhibiting higher IM power than that of mode 6 is an indication that switches S_3 and S_4 may have loose solder joints. Nevertheless, these results indicate that the degradation in IM performance due to the parasitic pixel layer switches is smaller as compared to the switches on parasitic patch layer, which was the case for EVM performance as well.

The performances of modes 1, 2 and 3 are expected to be similar, as for these modes the numbers of switches in ON state are very close (one for mode 1 and three for modes 2 and 3). However, while modes 1 and 3 exhibit similar IM performances with mode 1 performing slightly better as expected, the performance of mode 2 is surprisingly poorer. As in the case of mode 5, this relatively high difference between modes 2 and 3 can be attributed to the poor solder joints of parasitic pixel layer switches of mode 2 (S_3 and S_4), which is known to substantially increase the PIM power due to electro-thermal effects. The difference between modes 1 and 3 being very small indicates that the impact of ON-state parasitic pixel layer switches (S_1 and S_2) on IM performance is smaller than that of the single switch on microstrip feed line.

To further investigate the individual roles that the interconnecting switches and parasitic layers play on the IM performance, three additional modes (modes 11, 22, and 33) were again measured. Mode 11 with all switches in OFF state shows the smallest IM power, which is $\sim$-55dBc, as expected. Mode 33 with S_1 and S_2 being in ON state show very similar behavior to that of mode 11. Mode 22 exhibiting unexpectedly higher IM power in comparison to modes 11 and 33 is similar to the behavior of mode 2 in comparison to modes 1 and 3. Approximately 40 dB difference observed between legacy patch (IM= $\sim$-95 dBc) and the RA with all switches in OFF state (mode 11 with IM = $\sim$-55 dBc) can be attributed to the combined effects of the passive factors such as loose solder joints and electro-thermal effects, and large non-linear response of PIN diodes even in unpowered or reverse biased condition. Around 30 dB difference observed in IM powers between the best mode (mode 11) and the worst mode (mode 5) is due to the combination of the activations of non-linear switches and aforementioned passive factors. Also, it is worth noting that the impact of an ON-state switch on PIM can be higher than that of an OFF-state switch, as the ON-state switch current increases the electro-thermal effects.

The IM powers of modes 1 & 3 are $\sim$15 dB larger than those of modes 11 & 33. As the only difference between these two set of modes is S_6 being in ON state for modes 1 & 3, this 15 dB degradation can be attributed to the operation of S_6. As in the case of EVM, S_6 integrated on the feed layer, which is exposed to relatively higher RF power, plays a significant role on IM performance as well. The IM powers of modes 4, 5, and 6 ($\sim$ -28 $<$ IM $<$ $\sim$-35 dBc) indicate that the parasitic pixel layer switches play a relatively smaller role as compared to the twelve switches of the parasitic patch layer on IM performance.

Conclusion

Transceivers equipped with RAs performing concurrent configuration of impedance bandwidth and radiation pattern possess some key advantages. Characterization of such RAs using PIN diodes in terms of system level parameters such as error vector magnitude (EVM) and passive intermodulation product (PIM) is needed to determine the overall benefits of the RAs. For the presented RA, for all six modes of operations, the measured EVMs were less than -25 dBm (5.6%) for an input power of 30 dBm. These results revealed that the roles that both the number of switches and their locations in RA structure play

on EVM are equally important. The measured results for IM characterization reveal that the overall IM performance is contributed by the combined effects of the passive factors such as loose solder joints and electrothermal effects, and the inherit non-linear nature of PIN diodes. As the distortive effects on RA performance due to the inherit nonlinear nature of PIN diodes are unavoidable, it becomes important to minimize the effects resulting from non-linear passive factors such as loose solder joints and electro thermal effects. To this end, using effective multilayer printed circuit board manufacturing processes involving precise and high-yield pick/place procedures in mounting PIN diodes into the parasitic layers become critically important. The overall results showed that the parasitic pixel layer approach in implementing RAs is an effective approach as the degradation in EVM and PIM due to parasitic pixel layer switches is minimal.

3.2.3 MRA Design using Machine Learning Techniques

In this part, we revisit the MRA design using Genetic Algorithm (GA). With the GA, the relation between the switch states and the resulting radiation pattern is not taken into account. However, by learning the relation between the switch state, and parasitic layer geometry, one can create highly agile MRA designs in a faster approach. Thus, instead of randomly testing the patterns of each state, the algorithm can learn the way the candidate switch states shall be selected that would result in desired radiation pattern. In this work, our goal is to create artificial intelligence algorithms that can predict the behaviour of MRA using a limited set of MRA switch-radiation pattern tuples. In particular, we employ artificial neural networks (ANNs) to associate MRA states to resulting E-field radiation patterns. The use of ANN in RF systems have been previously investigated by the PI where a GaN HEMT power amplifier has been designed for a X-band [38].

Classification of E-field Patterns for MRAs

An electrical field of an EM wave is a vector valued complex field of 2D (we can ignore the radial component). E-field patterns can be expressed as smooth continuous functions of spherical coordinates, e.g.,

$$\vec{E}(\theta,\phi) = E_\theta(\theta,\phi)\hat{\theta} + E_\phi(\theta,\phi)\hat{\phi} \tag{9}$$

We can represent the E-field patterns using orthogonal basis patterns functions that can be obtained via orthogonalization techniques such as Gram-Schmidt process. We can also use compressed sensing techniques to generate sparse representation of E-fields using l_1-norm. In addition to these basis representations, we can employ similarity metrics that are of practical importance. For example, we can classify an E-field pattern according to its main direction according to its intensity. One such case includes 9 main directions (broadside, right, left, above/below horizon, and the 4 diagonal directions) where we quantize E-fields into the closest one of these 9 options. We can enrich the quantization sets by including additional spatial modes or polarization modes. The polarization modes can be defined in terms of axial ratio $\|E_\theta(\theta,\phi)\hat{\theta}/E_\phi(\theta,\phi)\|$

The main goal in representing the E-field in simple expressions is to reduce the learning space of a neural network and thus allow learning algorithm to focus on the features of interest that are practical and expected to provide gain in wireless applications relying on directional gains.

MRA States with Binary Switches

Association of inputs to outputs becomes easier if the input information is contained in a regularized format. For example, MRA states of a 12-switch parasitic layer (see Fig. 1) can be expressed as a 12×1 binary vector, $\boldsymbol{b} = [b_0 \dots b_{12}]$. This MRA has $2^{12} = 4096$ states. For MRA arrays, regardless of

representation of MRA states using binary vectors, each binary vector will result in a different parasitic layer geometry. However, using special representations, relation between binary vector representations and the physical geometry can be established in a tractable fashion in terms of both visually and analytically. In this regard, we can also represent all states as Cartesian product of two 6-state vectors, e.g., horizontal switch states, $\boldsymbol{h} = [h_0 \dots h_5]$, and $\boldsymbol{v} = [v_0 \dots v_5]$. With this representation, we have separated the two dimensions of the MRA parasitic layer representation into $64-$states. From previous sections, recall also that several states can be classified as rotationally similar since MRA geometry can be expressed as a simple axial rotation around the broadside of the array. Thus, vertical and horizontal switch states can be classified as similar states. We note that these features of the MRA greatly helps predicting the MRA patterns from switch states. The neural networks can utilize the axial rotation feature to associate MRA modes with similar geometry to E-field attributes. We would like to note that such observations in a much smaller scale have been made in earlier MRA designs based on Genetic Algorithms without any rigorous evaluation. In this study, we consolidate such associations using the much more powerful ANN tools.

Neural Network for MRA E-field Data

We are now ready to describe the neural network's learning method. We naturally land to a supervised learning approach where training sets are generated using the HFSS tool that can solve Maxwell Equations for a selected set of states. We employ both functional approximation (e.g., mean-square distance between the E-field patters in any basis domain) and pattern recognition approaches (k-neighbours neighbour algorithm). We note that we employ both approaches sine E-field representation has practical use in both approaches. On the one hand, we imagine the problem as an estimation of a discrete input ($\boldsymbol{b}$) - continuous output ($\vec{E}$) function. Alternatively, we can view $\|\vec{E}\|$ as 2D image in a (θ, ϕ) plane where we would like to classify the field into a pre-specified number of images. Once the ANN is trained with the available sets, the same network can be used to predict the radiation pattern for an untrained MRA states.

We note that training set is of critical importance for this problem. The training sets shall not contain rotatively symmetric states since they will give highly correlated information to the ANN and may not provide sufficient information for predicting the states with different caesaristic layer geometries.

Performance Study

A comprehensive report for the developed learning techniques is currently under preparation for submission to Transactions on Antennas and Prorogation [39].

3.2.4 Publications from the Project

2018-2019

Book chapters

[BC.1] Yanjun Pan, Ming Li, Yantian Hou, Ryan Gerdes, Bedri A. Cetiner, "Enhance Physical Layer Security via Channel Randomization with Reconfigurable Antennas," invited chapter in book Proactive and Dynamic Network Defense, Springer, ISBN: 978-3-030-10596-9, 2019

Refereed Journal Papers

[J.1] Ali Cafer Gurbuz and Bedri A. Cetiner, "CRLB Based Mode Selection and Enhanced DOA Estimation for Multifunctional Reconfigurable Arrays" Physical Communication, Vol. 38/100894, October

2019

[J.2] Md. A. Towfiq, A. Khalat, S. Blanch, J. Romeu, L. Jofre, and Bedri A. Cetiner, "EVM, IM and Radiation Characteristics of a Bandwidth and Pattern Reconfigurable Antenna," IEEE Antennas and Wireless Propagation Letters, vol. 18, No.10, pp: 1956-1960, October 2019.

[J.3] M. Hassan, I. Bahceci, T. Duman, and Bedri A. Cetiner, "Mode Shift Keying for Reconfigurable MIMO Antennas: Performance Analysis and Antenna Design", IEEE Trans. on Vehicular Technology, vol. 68, no.10, pp. 320-334, January 2019.

Conference Papers

[C.1] Germán Augusto Ramírez Arroyave, Javier Leonardo Araque Quijano, Sebastián Blanch Boris, Jordi Romeu Robert, Bedri A. Cetiner, Luis Jofre Roca "Study of interconnecting switch currents in reconfigurable parasitic layer antennas," IEEE Antennas and Propagation Symposium 2019

[C.2] Mehmet Tanagardi, Md Asaduzzaman Towfiq, Bedri A. Cetiner, "Radiation Pattern Reconfigurable Horn Antenna," IEEE Antennas and Propagation Symposium 2019

[C.3] Md Asaduzzaman Towfiq, Abdurazag Khalat, Bedri A. Cetiner, "High Gain Broadband Antenna for Point to Point Communication Systems," IEEE Antennas and Propagation Symposium 2019

2014-2018

Refereed Journal Papers

[J.4] Yanjun Pan, Yantian Hou, Ming Li, Ryan M. Gerdes, Kai Zeng, Md. A. Towfiq, Bedri A. Cetiner, "Message Integrity Protection over Wireless Channel: Countering Signal Cancellation via Channel Randomization," IEEE Trans. on Dependable and Secure computing, early access, 2018

[J.5] M. Hassan, I. Bahceci, and Bedri A. Cetiner, " Downlink Multi-user MIMO Transmission for Radiation Pattern Reconfigurable Antenna Systems," IEEE Trans. on Wireless Communications, vol. 17, no.10, pp. 6448-6463, October 2018.

[J.6] Md. A. Towfiq, I. Bahceci, J. Romeu, S. Blanch, L. Jofre, and Bedri A. Cetiner, " A Reconfigurable Antenna with Beam Steering and Beamwidth Variability for 5G Wireless Communication" IEEE Trans. on Antennas and Propagation, vol. 66, no.10, pp. 5052-5063, October 2018.

[J.7] A. Hossain, I. Bahceci, and Bedri A. Cetiner "Parasitic Layer Based Radiation Pattern Reconfigurable Antenna for 5G Communications," IEEE Trans. on Antennas and Propagation, vol. 65, no.12, pp. 6444-6452, December 2017

[J.8] I. Bahceci, M. Hassan, T. M. Duman and Bedri A. Cetiner, "Efficient Channel Estimation for Reconfigurable MIMO Antennas: Training Techniques and Performance Analysis," IEEE Trans. on Wireless Communications vol. 16, no.1, pp. 565-580, Jan. 2017. [J.9] Z. Li, I. Bahceci, and Bedri A. Cetiner, "A Broad-band beam-steering Reconfigurable Antenna," Microwave and Optical Technology Letters, Vol.59, No.1, pp.63-65, January 2017

Conference Papers

[C.4] Ali C. Gurbuz, Sevgi Z. Gurbuz, and Bedri A. Cetiner, "Cognitive Radar Utilizing Multifunctional

Reconfigurable Antennas," SPIE 2018

[C.5] Ali C. Gurbuz and Bedri A. Cetiner, "Multifunctional Reconfigurable Antennas for Cognitive Radars," IEEE Radar Conference 2018

[C.6] I. Bahceci, M. Hassan, and Bedri A. Cetiner, "Downlink Multi-User MIMO Transmission for Reconfigurable Antenna Systems," 2017 IEEE Wireless Communications and Networking Conference (WCNC)

[C.7] D. Joaquin and Bedri A. Cetiner, "A Low-Cost Microstrip Antenna Array for 60-GHz Applications," IEEE Antennas and Propagation Symposium 2016

[C.8] A. Towfiq, A. Khalat, and Bedri A. Cetiner, "Broadband High-Gain 60 GHz Antenna Array," IEEE Antennas and Propagation Symposium 2016

[C.9] A. Khalat, A. Towfiq and Bedri A. Cetiner "A 60 GHz Beam-Steering Reconfigurable Antenna," IEEE Antennas and Propagation Symposium 2016

[C.10] Rodrigo, D.; Romeu, J.; Cetiner, B.A.; Jofre, L, "Pixel Reconfigurable Antennas: Towards Low-Complexity Full Reconfiguration" EuCAP 2016

[C.11] E. Kaderli, I. Bahceci, K. M. Kaplan, B. A. Cetiner, "On the Use of Reconfigurable Antenna Arrays for DoA Estimation of Correlated Signals," IEEE Radar Conference 2016.

[C.12] Kurtulmaz, E.; Sahin, A.; Bahceci, I.; Cetiner, B.A., "Performance of MR antenna systems in IEEE 802.11ac network," in Signal Processing and Communications Applications Conference (SIU), 2015 23th , vol., no., pp.2419-2422, 16-19 May 2015, doi: 10.1109/SIU.2015.7130370

References

[1] Y. Pan, Y. Hou, M. Li, R. M. Gerdes, K. Zeng, M. A. Towfiq, and B. A. Cetiner, "Message integrity protection over wireless channel: Countering signal cancellation via channel randomization," *IEEE Transactions on Dependable and Secure Computing*, pp. 1–1, 2017.

[2] I. Bahceci and B. Cetiner, "Physical layer security for MU-MIMO communications using radiation pattern configurable antennas," *in preparation for IEEE Transactions on Wireless Communications*, 2020.

[3] ——, "Online reinforcement learning for joint channel estimation and MRA mode selection," *in preparation for IEEE Transactions on Wireless Communications*, 2020.

[4] ——, "A low-complexity hierarchical calibration technique for reconfigurable antenna arrays," *in preparation for IEEE Transactions on Antennas and Propagation*, 2020.

[5] M. Hasan, I. Bahceci, and B. Cetiner, "Improved constant envelope precoding for massive mimo systems using reconfigurable antennas," *in preparation for IEEE Transactions on Wireless Communications*, 2020.

[6] ——, "Joint analog and digital precoding for active antenna systems using MRAs," *in preparation for IEEE Transactions on Wireless Communications*, 2020.

[7] D. Sanchez-Hernandez and I. D. Robertson, "A survey of broadband microstrip patch antennas," *Microwave Journal*, vol. 39, no. 9, pp. 60–71, 1996.

[8] B. Yildirim and B. A. Cetiner, "Enhanced gain patch antenna with a rectangular loop shaped parasitic radiator," *IEEE Antennas and Wireless Propagation Letters*, vol. 7, pp. 229–232, 2008.

[9] F. Croq and D. M. Pozar, "Millimeter-wave design of wide-band aperture-coupled stacked microstrip antennas," *IEEE Transactions on antennas and propagation*, vol. 39, no. 12, pp. 1770–1776, 1991.

[10] G. V. Trentini, "Partially reflecting sheet arrays," *IRE Transactions on Antennas and Propagation*, vol. 4, no. 4, pp. 666–671, 1956.

[11] E. Nishiyama, M. Aikawa, and S. Egashira, "Stacked microstrip antenna for wideband and high gain," *IEE Proceedings-Microwaves, Antennas and Propagation*, vol. 151, no. 2, pp. 143–148, 2004.

[12] H. Yang and N. Alexopoulos, "Gain enhancement methods for printed circuit antennas through multiple superstrates," *IEEE Transactions on Antennas and Propagation*, vol. 35, no. 7, pp. 860–863, 1987.

[13] H. Attia, L. Yousefi, M. M. Bait-Suwailam, M. S. Boybay, and O. M. Ramahi, "Enhanced-gain microstrip antenna using engineered magnetic superstrates," *IEEE Antennas and Wireless Propagation Letters*, vol. 8, pp. 1198–1201, 2009.

[14] K. L. Chung and S. Chaimool, "Diamagnetic metasurfaces for performance enhancement of microstrip patch antennas," in *Proceedings of the 5th European Conference on Antennas and Propagation (EUCAP)*, April 2011, pp. 48–52.

[15] K. L. Chung, "Microwave antenna applications of metasurfaces," in *2015 International Workshop on Electromagnetics: Applications and Student Innovation Competition (iWEM)*, Nov 2015, pp. 1–4.

[16] S. Uda, "Wireless beam of short electric waves," *J. IEE*, pp. 273–282, 1926.

[17] M. A. Towfiq, I. Bahceci, S. Blanch, J. Romeu, L. Jofre, and B. A. Cetiner, "A reconfigurable antenna with beam steering and beamwidth variability for wireless communications," *IEEE Transactions on Antennas and Propagation*, vol. 66, no. 10, pp. 5052–5063, Oct 2018.

[18] HFSS, "Ansoft corp., pittsburgh, pa," 2015.

[19] Z. Liu, K. Boyle, J. Krogerus, M. de Jongh, K. Reimann, R. Kaunisto, and J. Ollikainen, "Mems-switched, frequency-tunable hybrid slot/pifa antenna," *IEEE Antennas and Wireless Propagation Letters*, vol. 8, pp. 311–314, 2009.

[20] M. Hamid, P. Gardner, P. S. Hall, and F. Ghanem, "Switched-band vivaldi antenna," *IEEE transactions on antennas and propagation*, vol. 59, no. 5, pp. 1472–1480, 2011.

[21] B. Cetiner, H. Jafarkhani, J.-Y. Qian, H. J. Yoo, A. Grau, and F. De Flaviis, "Multifunctional reconfigurable MEMS integrated antennas for adaptive MIMO systems," *IEEE Communications Magazine*, vol. 42, no. 12, pp. 62–70, 2004.

[22] F. A. Miranda, C. H. Mueller, and M. A. B. Meador, "Aerogel antennas communications study using error vector magnitude measurements," in *2014 IEEE Antennas and Propagation Society International Symposium (APSURSI)*, July 2014, pp. 1149–1150.

[23] G. H. Huff, N. Soldner, W. D. Palmer, and J. T. Bernhard, "Study of error vector magnitude patterns (evrp) for a transmit/receive pair of microstrip patch antennas," in *2006 IEEE Antennas and Propagation Society International Symposium*, July 2006, pp. 449–452.

[24] J. R. Wilkerson, I. M. Kilgore, K. G. Gard, and M. B. Steer, "Passive intermodulation distortion in antennas," *IEEE Transactions on Antennas and Propagation*, vol. 63, no. 2, pp. 474–482, Feb 2015.

[25] D. Wu, Y. Xie, Y. Kuang, and L. Niu, "Prediction of passive intermodulation on mesh reflector antenna using collaborative simulation: Multi-scale equivalent method and nonlinear model," *IEEE Transactions on Antennas and Propagation*, vol. PP, no. 99, pp. 1–1, 2017.

[26] X. Yuan, Z. Li, D. Rodrigo, H. S. Mopidevi, O. Kaynar, L. Jofre, and B. A. Cetiner, "A parasitic layer-based reconfigurable antenna design by multi-objective optimization," *IEEE Transactions on Antennas and Propagation*, vol. 60, no. 6, pp. 2690–2701, June 2012.

[27] *SMA100A Vector Signal Generator*, RHODE&SCHWARTZ, option: FSL-k91.

[28] *FSL-6 Spectrum Analyzer*, RHODE&SCHWARTZ, option: FSL-k91.

[29] M. D. McKinley, K. A. Remley, M. Myslinski, J. S. Kenney, D. Schreurs, and B. Nauwelaers, "Evm calculation for broadband modulated signals," in *64th ARFTG Conf. Dig*, 2004, pp. 45–52.

[30] *ZHL-16w-43+ High Power Amplifier*, Minicircuits.

[31] R. H. Caverly and G. Hiller, "Distortion in p-i-n diode control circuits," *IEEE Transactions on Microwave Theory and Techniques*, vol. 35, no. 5, pp. 492–501, May 1987.

[32] R. H. Caverly and G. Hiller, "Distortion in microwave and rf switches by reverse biased pin diodes," in *IEEE MTT-S International Microwave Symposium Digest*, June 1989, pp. 1073–1076 vol.3.

[33] R. Caverley, "A nonlinear pin diode model for use in multi-diode microwave and rf communication circuit simulation," in *1988., IEEE International Symposium on Circuits and Systems*. IEEE, 1988, pp. 2295–2299.

[34] *D313060 ISOLATION 18dB*, DITOM.

[35] *ZN2PD-9G-S+ Combiner*, Minicircuits.

[36] *ZADC-10-63-S+ Directional Coupler*, Minicircuits.

[37] *R&S FSLSpectrum Analyzer Specifications*, RHODE&SCHWARZ, 03 2013, version 11.00.

[38] Sang Yun Lee, B. A. Cetiner, H. Torpi, S. J. Cai, Jiang Li, K. Alt, Y. L. Chen, C. P. Wen, K. L. Wang, and T. Itoh, "An x-band gan hemt power amplifier design using an artificial neural network modeling technique," *IEEE Transactions on Electron Devices*, vol. 48, no. 3, pp. 495–501, March 2001.

[39] I. Bahceci and B. Cetiner, "Multifunctional and reconfigurable antenna design using artifical neural networks," *in preparation for IEEE Transactions on Antennas and Propagation*, 2020.